

# High CO<sub>2</sub> emissions through porous media: transport mechanisms and implications for flux measurement and fractionation

W.C. Evans<sup>a,\*</sup>, M.L. Sorey<sup>a</sup>, B.M. Kennedy<sup>b</sup>, D.A. Stonestrom<sup>a</sup>, J.D. Rogie<sup>c</sup>,  
D.L. Shuster<sup>b</sup>

<sup>a</sup> U.S. Geological Survey, 345 Middlefield Road, Menlo Park, CA 94025, USA

<sup>b</sup> Center for Isotope Geochemistry, Lawrence Berkeley National Laboratory, Berkeley, CA 94720, USA

<sup>c</sup> The Pennsylvania State University, 540 Deike Bldg., University Park, PA 16802, USA

Received 21 June 1999; accepted 15 April 2000

## Abstract

Diffuse emissions of CO<sub>2</sub> are known to be large around some volcanoes and hydrothermal areas. Accumulation-chamber measurements of CO<sub>2</sub> flux are increasingly used to estimate the total magmatic or metamorphic CO<sub>2</sub> released from such areas. To assess the performance of accumulation chamber systems at fluxes one to three orders of magnitude higher than normally encountered in soil respiration studies, a test system was constructed in the laboratory where known fluxes could be maintained through dry sand. Steady-state gas concentration profiles and fractionation effects observed in the 30-cm sand column nearly match those predicted by the Stefan-Maxwell equations, indicating that the test system was functioning successfully as a uniform porous medium. Eight groups of investigators tested their accumulation chamber equipment, all configured with continuous infrared gas analyzers (IRGA), in this system. Over a flux range of ~200–12,000 g m<sup>-2</sup> day<sup>-1</sup>, 90% of their 203 flux measurements were 0–25% lower than the imposed flux with a mean difference of -12.5%. Although this difference would seem to be within the range of acceptability for many geologic investigations, some potential sources for larger errors were discovered. A steady-state pressure gradient of -20 Pa/m was measured in the sand column at a flux of 11,200 g m<sup>-2</sup> day<sup>-1</sup>. The derived permeability (50 darcies) was used in the dusty-gas model (DGM) of transport to quantify various diffusive and viscous flux components. These calculations were used to demonstrate that accumulation chambers, in addition to reducing the underlying diffusive gradient, severely disrupt the steady-state pressure gradient. The resultant diversion of the net gas flow is probably responsible for the systematically low flux measurements. It was also shown that the fractionating effects of a viscous CO<sub>2</sub> efflux against a diffusive influx of air will have a major impact on some important geochemical indicators, such as N<sub>2</sub>/Ar, δ<sup>15</sup>N-N<sub>2</sub>, and <sup>4</sup>He/<sup>22</sup>Ne. Published by Elsevier Science B.V.

*Keywords:* CO<sub>2</sub>; Soil gases; Diffusion; Advection; Isotope fractionation

## 1. Introduction

Geoscientists have long used fumarole and hot-spring gases to infer subsurface conditions deep within volcanoes and hydrothermal systems, as re-

\* Corresponding author. Fax: +1-650-329-4463.  
E-mail address: wcevans@usgs.gov (W.C. Evans).

viewed by Chiodini and Marini (1998). The importance of diffuse degassing has only recently been recognized (Badalamenti et al., 1988; Baubron et al., 1990; Allard et al., 1991; Farrar et al., 1995; Bergfeld et al., 1998; Giammanco et al., 1998; Werner et al., 1998; Chiodini et al., 1999). The study of low-temperature, diffuse gas seepage provides a new monitoring and assessment tool, but forces researchers accustomed to sampling discrete vents to address problems related to gas flow through a porous medium, like soil or pumice.

Diffuse degassing studies often focus on the flow of CO<sub>2</sub> out of the soil, commonly (and herein) called CO<sub>2</sub> “flux” or “efflux” and expressed as (amount)(area<sup>-1</sup>)(time<sup>-1</sup>). Flux can be measured by placing accumulation chambers at discrete locations on the soil surface and monitoring the rate of CO<sub>2</sub> buildup in the chamber. This technique has been well studied in agricultural or ecological studies (e.g., Norman et al., 1997), where CO<sub>2</sub> is a product of soil respiration and is lost to the atmosphere by diffusion in a nearly 1:1 exchange with O<sub>2</sub> (Currie, 1970; Wood and Greenwood, 1971; Wood and Petraitis, 1984). However, a persistent efflux of CO<sub>2</sub> that is derived from some geologic source at depth presents a different situation; that is, a net outflow of gas. Such fluxes can also be much higher than those typically produced by soil respiration.

The present study arose, in part, to understand the data collected from the tree-kill areas on the flanks of Mammoth Mountain volcano in eastern California, USA. As first noted by Farrar et al. (1995), these areas comprise ~50 ha of forest, where following an inferred magmatic intrusion in 1989, the trees were killed by a huge efflux of CO<sub>2</sub> that caused high concentrations in the root zone. Several groups of researchers have since made accumulation-chamber flux measurements there but, in some cases, have reported total CO<sub>2</sub> emission rates that differ by a factor of two or three for the same tree-kill area (e.g., Farrar et al., 1998; Gerlach et al., 1998). To determine if these large differences could be attributed to problems with the accumulation chamber technique at high fluxes, a large, sand-filled cylinder was set up in the laboratory where flux could be measured at controlled CO<sub>2</sub> inflow rates.

An additional goal of this study was to examine the transport theory that applies to this apparently

widespread, if not common, geological occurrence: the diffusive inflow of air through a porous medium against an outflow of CO<sub>2</sub> that, at depth, is pressure-driven (commonly called an “advective” or “effusive” and herein called a “viscous” flux). This process was investigated by comparing the CO<sub>2</sub> profiles and compositional and isotopic fractionations estimated by transport theory to those observed within the sand column and, to some extent, at Mammoth Mountain (Evans et al., 1998; Sorey et al., 1998). Measured pressure profiles were used along with the “dusty gas” model (DGM) of Mason et al. (1967) to quantify the various components of flux. This DGM-based analysis of transport is presented here along with the results of the flux measurements.

## 2. Apparatus

### 2.1. Laboratory test system

A schematic of the laboratory test system, herein called the flux “bucket”, is shown in Fig. 1. It was similar in design to a setup recently described by Chiodini et al. (1998). It consisted of a standard 55-gal polyethylene drum, 56 ± 1 cm in diameter, cut to a height of 40 cm, with a perforated plastic disk supported 7 cm off the bottom. The thickness of the fill above the disk was varied between ~10 and

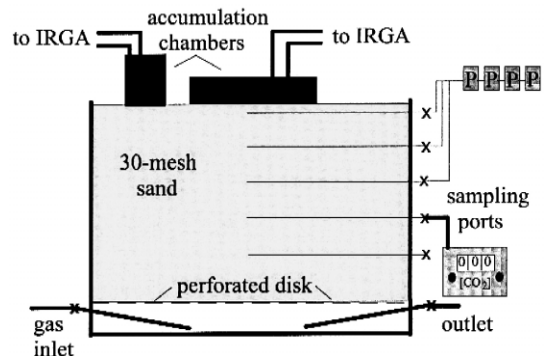


Fig. 1. Test apparatus consisting of 40-cm-high bucket, 56 cm in diameter; with gas inlet and (normally closed) outlet beneath 10–30 cm of sand supported on a perforated disk. Accumulation chambers were placed (singly) on the surface to measure flux. To study transport, pressure transducers (*P*) and portable CO<sub>2</sub> meters could sample different depths through fixed tubes. An “X” represents a valve, and inflow rate was measured at the inlet valve.

30 cm in different tests, but in all tests was 30-mesh, kiln-dried, beach sand. The surface area of the sand ( $0.25 \text{ m}^2$ ) was at least four times larger than the area (footprint) of any of the accumulation chambers tested. The intent of the large surface area was to mimic a natural soil without lateral boundaries.

It was assumed that the washed and graded Monterey sand was a suitable surrogate for the surficial deposits in the tree-kill areas on Mammoth Mountain. Those areas are uniformly covered by 0.1 to 0.4 m of 600-year-old Inyo pumice overlying Late Pleistocene, granitic, Tioga Till (a coarse, clean sand with scattered cobbles to boulders), typically well-drained and containing little leaf litter (see McGee and Gerlach, 1998). The sand is probably most similar to the pumice in terms of its characteristics as a porous medium, but certainly lacks the high internal porosity of the pumice.

Pure (99.99%)  $\text{CO}_2$  was admitted at constant flow through the gas inlet at rates set by an external pressure regulator and capillary restriction. For each regulator setting, the flow was determined by an in-line mass flow meter with 2% accuracy and/or by momentarily diverting the flow to a soap-bubble flow meter. Agreement between the two techniques was generally within 2%, but at flows above  $3000 \text{ g m}^{-2} \text{ day}^{-1}$ , only the soap-bubble flow meter could be used. The diurnal drift in the flow was as much as  $\pm 4\%$ , which presumably reflects the stability limit of the regulator. Laboratory air temperature was controlled at  $20 \pm 1^\circ\text{C}$ .

## 2.2. Flux measuring equipment

Gas flux can be measured in a number of different ways (Gurrieri and Valenza, 1988; Norman et al., 1997), but all systems tested here consisted of an accumulation chamber connected through a pump and tubing to an infrared gas analyzer (IRGA) with return flow of gas back to the chamber. The systems were manufactured by either LI-COR (Lincoln, NE) or West Systems (Pisa, Italy) or, in some cases, researchers employed user-built accumulation chambers and pumps attached to a LI-COR IRGA. The LI-COR IRGA has a fixed detector limit of 3000 ppm (at sea level pressure), while the Drager Polytron II IRGA used by West Systems has a variable limit that is normally set to several percent in high-flux situations.

Some of the systems used a fan to provide gas mixing within the chamber. Others used a specially designed manifold of inlet and outlet ports. Options on some LI-COR units included a caustic scrub feature, which allowed the initial concentration of  $\text{CO}_2$  to be reduced prior to measurement, and a gas-splitting device that allowed for longer measurement times at high fluxes. The West Systems units did not use a scrub feature. The larger range of the IRGA in this system obviated the need for gas splitting.

## 3. Methods

### 3.1. Flux measurement

Although each group of researchers customarily uses procedural details during flux measurement that are unique to that group, the basic technique and major variations can be summarized briefly. The inverted accumulation chamber is placed flat on the soil surface or pre-installed collar to trap the outflow of  $\text{CO}_2$ . In these tests, the chambers fit to the sand surface without any gaps, so that pre-installed collars were not used. The rise in the concentration of  $\text{CO}_2$  with time,  $d[\text{CO}_2]/dt$ , is combined (assuming ideal gas behavior) with the volume ( $V$ ) and footprint ( $A$ ) of the chamber and its internal temperature ( $T$ ) and pressure ( $P$ ) to calculate flux ( $\Phi$ ):

$$\Phi = \frac{PV}{RTA} (d[\text{CO}_2]/dt), \quad (1)$$

where  $R$  is the gas constant, and units can be chosen to give  $\Phi$  in  $\text{g m}^{-2} \text{ day}^{-1}$ . Successful application of Eq. (1) requires a determination of  $d[\text{CO}_2]/dt$  at a time when  $[\text{CO}_2]$  gradients are minimally disturbed by the presence of the chamber.

At any flux, the steady  $[\text{CO}_2]$  buildup within the chamber reduces the  $[\text{CO}_2]$  gradient in the soil, slowing the diffusive transport of  $\text{CO}_2$  across the soil–air interface, and causing a decrease in  $d[\text{CO}_2]/dt$ . Consequently, many previous studies of  $\text{CO}_2$  flux have reported that accumulation chambers can underestimate flux in soil respiration studies (e.g., Nay et al., 1994). Healy et al. (1996) reviewed this topic and calculated the chamber effects on diffusive transport under a number of different theo-

retical conditions. Other researchers have developed a method to use the curvature in  $d[\text{CO}_2]/dt$  during long measurement intervals to determine the undisturbed gas flux (e.g., Anthony et al., 1995).

To circumvent the problem of altering the soil  $[\text{CO}_2]$  gradient, LI-COR developed the protocol of pre-scrubbing the  $\text{CO}_2$  in the chamber to less than ambient levels and then taking the slope of  $d[\text{CO}_2]/dt$  when chamber  $[\text{CO}_2]$  was equal to ambient  $[\text{CO}_2]$ . The effect of the chamber on the soil  $[\text{CO}_2]$  gradient should be minimal at this time (Norman et al., 1997; Welles et al., 2000). However, Chiodini et al. (1998) argued that at high fluxes,  $d[\text{CO}_2]/dt$  is sufficiently linear for a long enough time that flux can be determined without pre-scrubbing.

### 3.2. Gas sampling and analysis

The profile of  $[\text{CO}_2]$  in the sand was determined by portable gas meters manufactured by Dräger (0–100%  $\text{CO}_2$ ) and Bacharach (0–60%  $\text{CO}_2$ ). Each had internal pumps to draw gas through an internal IRGA. The meters were frequently calibrated with several  $\text{CO}_2$  standards covering the range of interest. Uncertainties in the readings were generally  $< 3\%$ . Normally, the  $[\text{CO}_2]$  profile was determined at different times from the flux measurements, but in a special test focusing on chamber effects (discussed later), the profile was monitored during deployment of an accumulation chamber on the sand surface.

One gas sample was collected from within the sand into a pre-evacuated 150-cm<sup>3</sup> pyrex bulb. This sample was analyzed by gas chromatography for bulk composition, and a split of the gas was purified for N-isotope analysis. A separate sample used for noble gas analysis was collected in a 10-cm<sup>3</sup> copper tube sealed by clamps at both ends. These collection procedures were similar to those often used to collect gas from the soils at Mammoth Mountain and other field locations. Details of the analytical procedures have been reported elsewhere (Kennedy et al., 1985; Evans et al., 1988; Hiyagon and Kennedy, 1992).

### 3.3. Pressure measurements

Pressure profiles were investigated using transducers with a full-scale range of  $\sim 1$  kPa calibrated

against an inclined water manometer and mounted in a horizontal bank within an insulated container. Data were collected and stored at 1-min intervals. It was assumed that the composition of the gas in the tubes connecting the sand bucket to each transducer was the same as that measured at the sampled depth.

## 4. Results

### 4.1. Fluxes

The results of 203 accumulation chamber measurements are shown in Fig. 2. These results do not include any flux measurements made when equipment or technique was deliberately altered to investigate the magnitude of resultant errors or when equipment was found to have possible mechanical or calibration problems. The tests covered a flux range of 200–12,400  $\text{g m}^{-2} \text{ day}^{-1}$ . The dashed regression line on Fig. 2 shows that over the entire flux range, measured fluxes are in reasonable agreement with imposed fluxes, but do exhibit a small negative bias. Overall, 94% of the measured fluxes were 0–30% lower, and 6% were 0–10% higher, than the imposed flux. The mean difference was  $-12.5\%$ .

Fig. 3 shows the detailed results of one of the flux tests when five different groups of investigators participated. These results are fairly typical of all the tests; only 1 in 20 measurements exceeded the im-

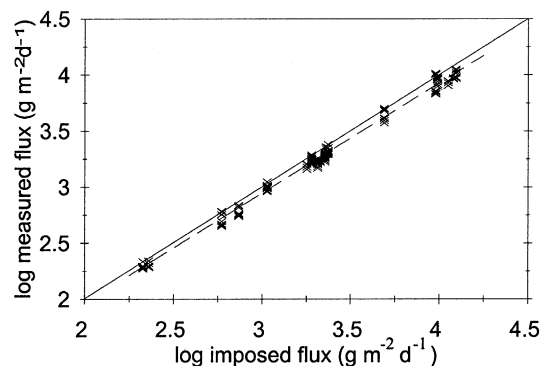


Fig. 2. Log–log comparison of 126 flux measurements to the imposed flux (solid line). The imposed fluxes were calculated from the measured  $\text{CO}_2$  inflow rate, normalized to the 0.25-m<sup>2</sup> surface area of the sand. Dashed line is regression line through data ( $R^2 = 0.996$ ).

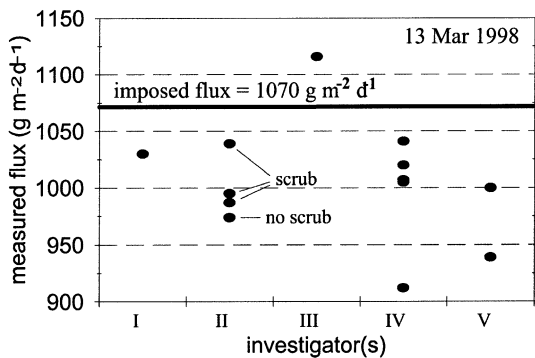


Fig. 3. Results obtained with five different accumulation chamber systems at a single imposed flux of  $1070 \text{ g m}^{-2} \text{ day}^{-1}$ .

posed flux. Some of these investigators used the caustic scrub technique. As noted on Fig. 3, group II used the scrub for three measurements and then made a fourth measurement without a scrub. This test also involved groups using the largest and smallest, and shortest and tallest chambers investigated in this entire study. Tests on other dates provided comparisons of vented vs. nonvented chambers. None of these variations in equipment or protocol seemed to produce large differences in the flux measurements.

The tests essentially covered the range of interest at Mammoth Mountain. Some measured fluxes there exceed  $12,400 \text{ g m}^{-2} \text{ day}^{-1}$ , but the areas where this occurs are small and contribute little to the total flux from an entire tree-kill area (Farrar et al., 1998). Similarly, the contribution from areas where the flux is  $< 200 \text{ g m}^{-2} \text{ day}^{-1}$  is not a large fraction of the total flux (Gerlach et al., 1998). Although the reasons for discrepant total  $\text{CO}_2$  emission rates at Mammoth Mountain were not resolved, potential sources of error in flux measurement were identified.

Adequate mixing of gas within the accumulation chamber, by either a mixing manifold or a fan, is important over this flux range. Tests of the fan-equipped units showed that the  $d[\text{CO}_2]/dt$  plot had more random noise and curvature if the fan was off. Another problem was that  $d[\text{CO}_2]/dt$  plots occasionally showed a rapid jump in the first few seconds after the chamber was set, before changing to a line of the correct slope. This effect was attributed to an observed enrichment of  $\text{CO}_2$  in the air layer just above the sand surface. Setting the chamber disturbs the layering of this air, giving an initial rate of  $[\text{CO}_2]$

increase that does not reflect the steady-state efflux from the sand. A bigger problem arose at fluxes near  $10^4 \text{ g m}^{-2} \text{ day}^{-1}$ : the  $d[\text{CO}_2]/dt$  plot can sometimes show pronounced curvature until  $[\text{CO}_2]$  in the chamber exceeds several thousand ppm. Large (up to 50%) positive or negative errors can result if investigators fail to recognize either of these problems in  $d[\text{CO}_2]/dt$  plots. Overly disturbing the sand surface when setting the chamber can also produce either positive or negative errors, with the magnitude dependent on the amount of disturbance.

Identifying the optimal procedure was not the goal of this study, but we can offer the following observations on measurement of high fluxes. Pre-scrubbing is substantially more difficult at high fluxes, and seemingly less important to the final value, than at low fluxes. A large detector range or flow splitting seems more useful, so that effects of chamber emplacement and the shape of  $d[\text{CO}_2]/dt$  can be better discerned. This would allow an initial mixing of a  $\text{CO}_2$ -rich stagnant surface layer to be identified, and permit more complex flux equations, such as that proposed by Welles et al. (this volume), to be evaluated. Investigators should avoid disturbing the natural soil surface and carefully consider whether collars are needed in their field areas. Satisfactory measurements of flux were made here in the sand without using collars. Finally, it is strongly recommended that investigators periodically check their flux measuring equipment in a laboratory test system like the one described here. In using the sand bucket, many mechanical or calibration problems with the flux measuring equipment were only discovered after finding a large disagreement between measured and imposed fluxes.

The flux results obtained here are in reasonable concordance with the those of Chiodini et al. (1998), who tested a West Systems package over a similar range of fluxes and reported that measurements were within 15% of the imposed flux. However, those authors do not mention a systematic bias to low values as was found here. The bias could be caused by a problem with the bucket (e.g., a nonuniform flux over the sand surface) or to factors common to the flux measuring systems (e.g., pumping rate or detector speed not able to keep up with  $d[\text{CO}_2]/dt$  in the chamber. However, measured fluxes were lower regardless of whether the accumulation cham-

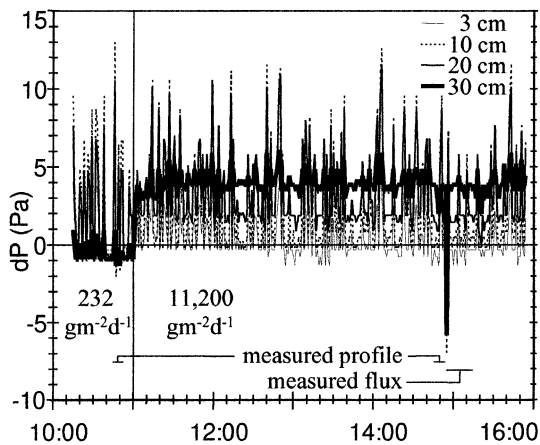


Fig. 4. Pressure records from four horizontally mounted transducers at two fluxes, 232 and 11,200  $\text{g m}^{-2} \text{ day}^{-1}$ . The transducer reference was ambient laboratory air pressure, but an offset is possible due to height differences between the transducers and bucket.

bers were placed in the center or near the edge of the sand surface, ruling out nonuniform flux as a serious source of error. Two of the flux measuring systems were tested directly by disconnecting the gas inlet tube from the bucket and setting the accumulation chamber over the end of the tube on an impermeable mat. In 18 of these measurements over a range of fluxes, the mean difference between measured and imposed fluxes was only  $-3.3\%$  (vs.  $-16.7\%$  on the sand for these same two (West) systems). Thus, the pumping rates and detector speeds were adequate. The systematic bias of measured fluxes to be less than imposed fluxes seems to reflect some impact of the accumulation chamber on gas flow through the sand.

#### 4.2. Pressures

Pressure gradients were extremely small due to the high permeability of the sand. Fig. 4 shows the pressures measured by four transducers connected to tubes from 3, 10, and 20 cm depth in the sand and to the outlet tube (30 cm). Even though the transducers used were among the most sensitive available, the small pressure gradient allows the quantization limit of the data logger to be apparent ( $\sim 0.5$  Pa) in Fig. 4. The large positive spikes ( $\sim 5$  Pa) reflect fluctuations in ambient laboratory air pressure, to which all

transducers were referenced, due to changes in laboratory ventilation and air flow. The 10 and 20 cm depths show a bigger effect than the 3 cm depth because they are more isolated from the ambient pressure by the sand. At 30 cm depth, the ambient pressure fluctuations are apparently lessened by feedback through the regulator on the  $\text{CO}_2$  tank, which was also referenced to ambient pressure. Such fluctuations are not likely to significantly alter gas flow through the regulator, which was set at delivery pressures of  $10^4$ – $10^6$  Pa above ambient.

Despite the noise, a baseline can be identified for the transducer readings. At the lower flux ( $232 \text{ g m}^{-2} \text{ day}^{-1}$ ), the baselines of all transducers are less than ambient. This likely reflects the calibration bias of the transducers at their installed location. The steady-state pressure gradient is below detection. At the higher flux ( $11,200 \text{ g m}^{-2} \text{ day}^{-1}$ ), a steady-state pressure gradient of  $\sim -4$  Pa across 30 cm is readily discernable. The pressure dip at 14:55 occurred at the start of a series of six accumulation chamber measurements but cannot be attributed to any identifiable action. Fig. 4 demonstrates that a tiny pressure gradient is sufficient to drive a huge flux. This tiny gradient can be easily overwhelmed by externally imposed pressure changes.

#### 4.3. $\text{CO}_2$ profiles

At any given flux, the  $[\text{CO}_2]$  gradients were identical regardless of whether they were measured at the center or next to the edge of the bucket. This is demonstrated in Fig. 5 for an imposed flux of 2200 g

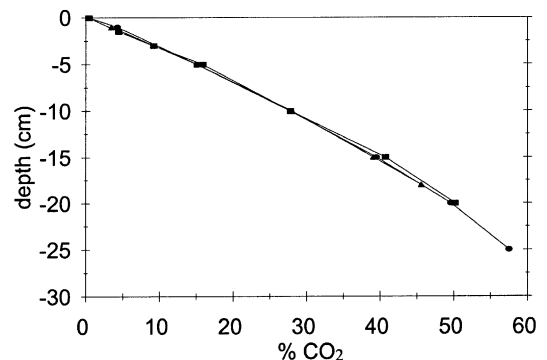


Fig. 5. Profiles of  $[\text{CO}_2]$  determined by portable gas meter near the edge of the sand and at two interior locations at the constant flux of  $2200 \text{ g m}^{-2} \text{ day}^{-1}$ .

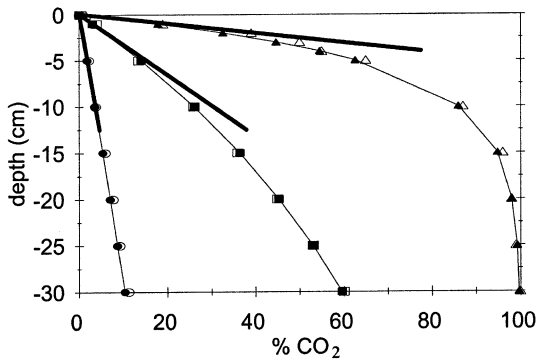


Fig. 6. Profiles of  $[\text{CO}_2]$  determined by portable gas meter (open symbols) and calculated using Eq. (6) in text (filled symbols) at three imposed fluxes: ellipses,  $229 \text{ g m}^{-2} \text{ day}^{-1}$ ; rectangles,  $1900 \text{ g m}^{-2} \text{ day}^{-1}$ ; and triangles,  $12,400 \text{ g m}^{-2} \text{ day}^{-1}$ . Three heavy lines represent the  $[\text{CO}_2]$  gradient expected from Eq. (3) assuming that near-surface  $\text{CO}_2$  transport is entirely by Fickian diffusion.

$\text{m}^{-2} \text{ day}^{-1}$ . This provides additional evidence that preferential channeling of  $\text{CO}_2$  flow along the inner walls of the bucket was insignificant.

The overall shape of the  $[\text{CO}_2]$  gradient depends on the imposed flux. Three representative profiles are shown (open symbols) in Fig. 6 for imposed fluxes that essentially span the range of the tests. The profile changes from nearly linear at  $229 \text{ g m}^{-2} \text{ day}^{-1}$  to moderately curved at  $1900 \text{ g m}^{-2} \text{ day}^{-1}$  to highly curved at  $12,400 \text{ g m}^{-2} \text{ day}^{-1}$ . In discussing similar profiles, Gurrieri and Valenza (1988) note that this trend represents the change from mainly diffusive to mainly viscous  $\text{CO}_2$  flow at the base of the profile. For all three fluxes, it was possible to detect a  $[\text{CO}_2]$  higher than in normal air many cm above the sand (as discussed above). The interfacial values at  $z = 0 \text{ cm}$  (0.08%, 0.26%, and 1.5%, respectively), measured by holding the detector inlet at the sand surface, varied with the amount of air motion around the bucket but were reasonably stable during the course of a measurement.

## 5. Discussion

Before attempting to explain the bias in the flux results and the shape of the  $[\text{CO}_2]$  profiles, a discussion of pressure-driven gas transport through a porous medium is needed. This discussion of transport fol-

lows that of Thorstenson and Pollock (1989a,b), who developed a procedure to calculate the different flux components in soil using the dusty-gas model (DGM). Their example of a  $\text{CH}_4$  flux from a source at depth is particularly relevant to our study, the main difference being that  $\text{CO}_2$  is heavier than air.

### 5.1. Gas transport calculations

In these tests, gas transport is driven by gradients in both pressure (Fig. 4) and concentration (Fig. 6). These are not independent quantities; the gradient in one is linked (through the properties of the medium) to a specific gradient in the other (Mason et al., 1967). Nevertheless, it is possible to mathematically distinguish the fraction of the  $\text{CO}_2$  flux that is pressure-driven (the viscous component) from the fraction that is concentration-driven (the diffusive component). For gases, the intermolecular distance is not necessarily trivial compared to the finite pore size in porous media, resulting in some gas flow by Knudsen diffusion, where molecule-medium collisions predominate over intermolecular collisions. Therefore, Darcy's law and Fick's law do not exactly govern the viscous and diffusive fluxes.

Fickian diffusion is described by:

$$-J_{\text{CO}_2} = n_a \tau D (d[\text{CO}_2]/dz), \quad (2)$$

where  $J$  is flux (negative up out of the sand),  $n_a$  is air-filled porosity,  $\tau$  is tortuosity,  $D$  is the diffusion coefficient, and  $z$  is depth. For mixing between  $\text{CO}_2$  and air, the binary diffusion coefficient  $D_{\text{CO}_2-\text{N}_2}$  can be used in Eq. (2) without appreciable error. The measured  $n_a$  of the sand was 0.40. There are several empirical (non-DGM) formulas for estimating  $\tau$  (see Abu-El-Sha'r and Abriola, 1997), but at this  $n_a$ , Currie (1970) showed that for dry sand,  $n_a \tau = n_a^{3/2}$ , and Eq. (2) becomes:

$$-J_{\text{CO}_2} = 0.25 D_{\text{CO}_2-\text{N}_2} (d[\text{CO}_2]/dz), \quad (3)$$

For any given  $-J_{\text{CO}_2}$ , the  $[\text{CO}_2]$  gradient ( $d[\text{CO}_2]/dz$  or  $\nabla \text{CO}_2$ ) can be calculated.

The  $[\text{CO}_2]$  gradients calculated using  $D = 0.15972$  (Marrero and Mason, 1972) and setting  $-J_{\text{CO}_2}$  equal to the three imposed fluxes are shown as heavy straight lines extending down from the sand surface in Fig. 6. In plotting each line, the  $[\text{CO}_2]$  at

$z = 0$  was set equal to the measured interfacial value. That the calculated  $\nabla\text{CO}_2$  matches the initial slope of the observed profiles well (within 10%) shows that  $\text{CO}_2$  transport across the sand–air interface is mainly by Fickian diffusion (surface effects are ignored herein).

To further investigate transport, a DGM-based equation must be considered. For  $v$  components:

$$\sum_{j=1, j \neq i}^v \frac{X_i N_j^T - X_j N_i^T}{n_a \tau D_{ij}} - \frac{N_i^T}{D_i^K} = \frac{P \nabla X_i}{RT} + \left\{ 1 + \frac{B_k P}{D_i^K \mu} \right\} \frac{X_i \nabla P}{RT}, \quad (4)$$

where the  $X_i$  are mole fractions,  $N_i^T$  are the total molar fluxes,  $D_i^K$  are the Knudsen diffusivities, of each component  $i$ ;  $D_{ij}$  are the binary diffusion coefficients for  $i$  and  $j$ ,  $B_k$  is permeability, and  $\mu$  is viscosity of the gas mixture. (The derivation and discussion of this equation can be found in Thorsten and Pollock, 1989a.)

The good agreement with Fick's law demonstrated in Fig. 6 suggests that Knudsen diffusion is not a significant factor here. As in most dry soils, the Knudsen diffusivities are orders of magnitude larger than the effective binary diffusivities, and the term on the left-hand side of Eq. (4) with  $D_i^K$  in the denominator can be ignored for many purposes. In our tests,  $\nabla P$  was  $\leq 20$  Pa/m, and Fig. 6 shows that  $\nabla X_i$  were large. For reasonable values of  $B_k$  and  $D_i^K$ , the last term can also be ignored,  $P$  can be taken as constant, and Eq. (4) reduces to the Stefan–Maxwell equations:

$$\nabla X_i = \frac{RT}{P} \sum_{j=1, j \neq i}^v \frac{X_i N_j^T - X_j N_i^T}{n_a \tau D_{ij}}. \quad (5)$$

For the “stagnant” air gases (in this case, including  $\text{O}_2$  as no respiration occurs), the downward diffusive flux of each species,  $N_i^D$ , is exactly balanced at each depth by an upward viscous flux,  $-N_i^V$ ;  $N_i^T = N_i^D + N_i^V = 0$ , and Eq. (5) integrates to:

$$X_i = X_{i,z=0} e^{(zRTN_{\text{CO}_2}^T / P n_a \tau D_{i-\text{CO}_2})}. \quad (6)$$

Using Eq. (6), the mole fraction of each of the air gases can be calculated as a function of depth and total  $\text{CO}_2$  flux ( $N_{\text{CO}_2}^T$  is a negative number so  $X_i$

decrease with depth). The mole fraction of  $\text{CO}_2$  can then be calculated by the difference,  $X_{\text{CO}_2} = 1 - \sum X_i$ . The  $[\text{CO}_2]$  values calculated by setting  $-N_{\text{CO}_2}^T$  equal to the imposed fluxes are shown as solid symbols in Fig. 6. The agreement between measured and calculated  $[\text{CO}_2]$  is remarkable. The good agreement argues against any significant channeling of  $\text{CO}_2$  flow along the inside edge of the bucket, in which case, calculated  $[\text{CO}_2]$  would exceed measured values at each depth. In measuring the profiles, the gas detectors needed to withdraw  $\geq 50$  cm<sup>3</sup> of gas to provide a stable  $[\text{CO}_2]$  reading, and thus sampled a depth interval ( $\Delta z$ ) rather than a discrete depth. For the shallowest part of the 12,400 g m<sup>-2</sup> day<sup>-1</sup> profile where  $\nabla\text{CO}_2$  is greatest, the poorer agreement between measured and calculated  $[\text{CO}_2]$  could, in part, reflect the fact that  $\Delta z/z$  was large.

## 5.2. Fractionation effects

Because the vertical distribution of each compound or isotope can be calculated separately using Eq. (6), the fractionation in compound or isotope ratios can also be calculated. Alternatively, for calculating the ratio of any two species  $i$  and  $j$ , Eq. (6) can be expressed as:

$$\ln(X_i/X_{i,z=0}) = (D_{j-\text{CO}_2}/D_{i-\text{CO}_2}) \ln(X_j/X_{j,z=0}), \quad (7)$$

and as pointed out by Severinghaus et al. (1996), equations like Eq. (7) allow fractionations to be calculated independent of most of the parameters in Eq. (6). This is particularly useful for evaluating soil gases in field situations because uncertainties in  $z$  (or  $\Delta z$ ) and natural variations in  $n_a$  and  $\tau$  need not be considered. Also, whereas individual  $D_{i-\text{CO}_2}$  are very sensitive to  $P$  and  $T$ , the ratio of diffusion coefficients in Eq. (7) is relatively insensitive over the small range of  $P$  and  $T$  expected within a typical soil column a few meters thick. Although Eq. (7) is independent of flux magnitude, in field situations, it will only be valid where a net  $\text{CO}_2$  flux from some geologic source at depth overwhelms soil respiration fluxes.

Eq. (7) can be used to calculate the abundance of all air species as a function of  $[\text{CO}_2]$ . For example, if at some depth  $z$ ,  $X_{\text{CO}_2} = 0.8$ , then  $X_a/X_{a,z=0}$  is set

equal to 0.2 for any air species *a*, and  $X_i/X_{i,z=0}$  for all other species calculated. The value of  $X_a/X_{a,z=0}$  is then modified so that the sum of all gases is 1.0. This procedure converges after two to three iterations. Table 1 compares the results of the calculations at  $X_{CO_2} = 0.806$  to an analysis of gas collected from  $9 \pm 1$  cm depth during the  $12,400 \text{ g m}^{-2} \text{ day}^{-1}$  test profiled in Fig. 6.

The calculated trends in various ratios are shown in Figs. 7 and 8 as a function of  $[CO_2]$ . For the ratios of  $^{29}N_2/^{28}N_2$ ,  $N_2/Ar$ ,  $^4He/^{36}Ar$ ,  $^{22}Ne/^{36}Ar$ , and  $^{84}Kr/^{36}Ar$ , the measured fractionation between light and heavy species is slightly less than expected at  $X_{CO_2} = 0.806$ . Possible explanations for this small discrepancy include: (a) the small concentration dependence of  $D_{i-CO_2}$  (see Marrero and Mason, 1972) was ignored over this extreme range of composition; (b) Knudsen diffusion was ignored in the simplification of Eq. (4) to Eqs. (5)–(7); and (c) the impact of gas removal during sampling was not addressed. In

Table 1  
Calculated and measured gas characteristics

Species or ratio	Measured in sample	Calculated from Eq. (6)	$D_{i-CO_2}$ ( $\text{cm}^2 \text{ s}^{-1}$ )
vol.% He	$0.0003 \pm 0.0001$	0.0003	0.57973
vol.% Ar	$0.164 \pm 0.001$	0.1590	0.14770
vol.% O <sub>2</sub>	$4.052 \pm 0.008$	4.029	0.15854
vol.% N <sub>2</sub>	$15.17 \pm 0.03$	15.20	0.15972
vol.% CO <sub>2</sub>	$80.6 \pm 0.4$	$\equiv 80.6$	–
N <sub>2</sub> /Ar	92.4	95.6	–
N <sub>2</sub> /O <sub>2</sub>	3.744	3.770	–
$\delta^{15}N-N_2$	$-14.0 \pm 0.1\text{‰}$	$-17.4\text{‰}$	0.15804 ( $^{29}N_2$ )
$F(^4He)$	$3.54 \pm 0.18$	3.56	0.57973 ( $^4He$ )
$F(^{22}Ne)$	$1.77 \pm 0.04$	1.96	0.24995 ( $^{22}Ne$ )
$F(^{84}Kr)$	$0.606 \pm 0.012$	0.508	0.10902 ( $^{84}Kr$ )
$F(^{132}Xe)$	$0.466 \pm 0.025$	0.303	0.08972 ( $^{132}Xe$ )

Bulk compositions and ratios from gas chromatography and isotopic ratios from mass spectrometry. The  $F(i)$  notation means  $(i/^{36}Ar)/(i/^{36}Ar)_{air}$  where  $i$  is  $^4He$ ,  $^{22}Ne$ ,  $^{84}Kr$ , or  $^{132}Xe$ . Binary diffusion coefficients (at 293 K) are from Marrero and Mason (1972) except for Kr (Kestin and Yata, 1968) and Xe (Perry and Green, 1984; pp. 3–285). Uncertainties in the coefficients are estimated to be 2–3% for all species except Xe. The use of more significant figures here allows the isotopic effects to be shown. Values of  $D_{i-CO_2}$  for specific isotopes were calculated using  $D/D^* = \{[(M_i + 44)/(M_i \times 44)]/[(M_i^* + 44)/(M_i^* \times 44)]\}^{1/2}$  where  $M_i^*$  is the molecular weight of the specific isotope and  $M_i$  is the molecular weight of the naturally occurring substance  $i$  (see Marrero and Mason, 1972; Severinghaus et al., 1996). The value of  $D_{Ar-CO_2}^{36}$  is 0.15193.

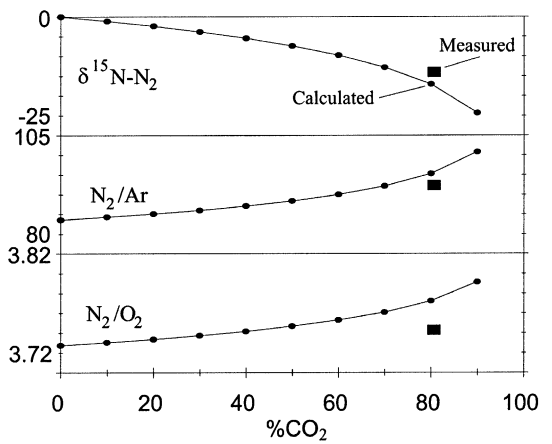


Fig. 7. Fractionation in various gas ratios expected from Eq. (7) as a function of  $[CO_2]$  at 10% increments (ellipses). Ratios measured in gas collected from sand during  $12,400 \text{ g m}^{-2} \text{ day}^{-1}$  flux test are shown by rectangles.

light of these and other possible errors, the agreement between measured and calculated values is remarkably close.

For Xe, the binary diffusion coefficient  $D_{Xe-CO_2}$  is not as well known, possibly explaining the slightly larger discrepancy for  $^{132}Xe/^{36}Ar$  in Fig. 8. For  $N_2/O_2$ , the small difference in  $D_{N_2-CO_2}$  and  $D_{O_2-CO_2}$  leads to a very small calculated fractionation between these two species, even at high  $[CO_2]$ . The greater apparent discrepancy between measured and calculated values for  $N_2/O_2$  (Fig. 7) may, in

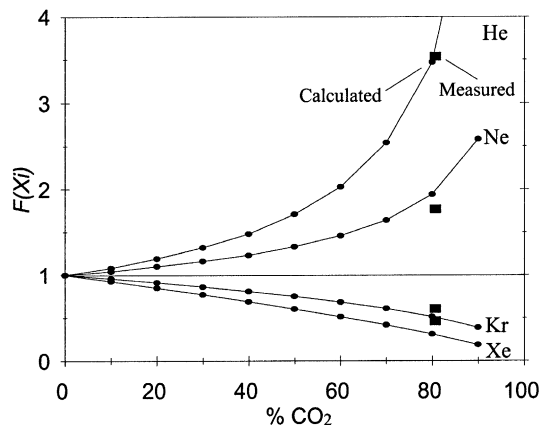


Fig. 8. Fractionation of  $^4He$ ,  $^{22}Ne$ ,  $^{84}Kr$ , and  $^{132}Xe$  relative to  $^{36}Ar$  and normalized to air (see Table 1). Symbols as in Fig. 7.

part, reflect the limits of precision of gas chromatography.

In volcanic or hydrothermal gas studies, the ratios of  $N_2/Ar$  and  $N_2/O_2$  are commonly measured in mofettes and fumarolic vents. Values of  $N_2/Ar$  greater than the air ratio (83.6) are usually assumed to indicate some nonatmospheric  $N_2$ , which is then investigated using  $\delta^{15}N-N_2$  (e.g., Minissale et al., 1997). Fig. 7 shows the problems that can arise in areas of diffuse  $CO_2$  flux: enrichments in  $N_2/Ar$  and large depletions in  $\delta^{15}N-N_2$  occur simply as a result of diffusive fractionation of air. Very negative  $\delta^{15}N-N_2$  values (to  $-6\%$  relative to air) were reported by Sorey et al. (1998) for Mammoth Mountain soil gases containing 80–95%  $CO_2$ . This  $N_2$  is simply fractionated air, not  $N_2$  from some deep source. In a fumarole there, where the trace of  $N_2$  (1% of total gas) does reflect a geologic source,  $\delta^{15}N-N_2$  is  $+1.5\%$  relative to air.

The highly fractionated  $F(^{22}Ne)$  values (to 1.6) reported in Mammoth Mountain soil gases (Sorey et al., 1998) can also be accounted for by Eq. (7). In fumarolic vents, it is generally assumed that He and Ne are not greatly fractionated during gas transport and phase separation. However, fractionations like those in Fig. 8 may need serious consideration when correcting soil–gas  $^3He/^4He$  ratios for air contamination based on He/Ne ratios. In contrast, the ratio of  $N_2/O_2$  is minimally affected by diffusive fractionation because  $D_{O_2-CO_2}$  and  $D_{N_2-CO_2}$  are nearly equal. For this reason, changes in  $N_2/O_2$  mainly reflect  $O_2$  consumption in the soil and can be used to quantify the small respiration component in areas of high  $CO_2$  flux. Using this method at Mammoth Mountain, Farrar et al. (1995) demonstrated good agreement with the  $^{14}C$  results.

### 5.3. Viscous flux

Although  $CO_2$  transport across the interface at even the highest fluxes is described well by Fickian diffusion, and fractionation effects at all depths are constrained solely by diffusivities in Eq. (7), it is important to remember that the concentration profiles (i.e., in Fig. 6) are established by a pressure-driven flow of gas through the system. This discussion of transport differs from that of Gurrieri and

Valenza (1988), who focused on  $CO_2$  transport, in that we are considering transport of all the air gases as well. The total viscous flux of gas does not diminish near the sand surface as  $CO_2$  transport becomes diffusive, it changes in chemical composition. What begins as a viscous flux of  $CO_2$  at the base of the sand becomes a viscous flux of mainly air near the sand surface. In consequence, pressure gradients persist up to the sand surface where accumulation chambers are placed.

Calculating the viscous flux requires that permeability and Knudsen diffusivities be known or estimated and may not be practical in many field studies. We summarize the process here so that accumulation chamber effects on the pressure gradient can be considered. Thorstenson and Pollock (1989a) show that the viscous flux ( $N^V$ ) can be calculated in the DGM according to:

$$N^V = \frac{\sum_{i=1}^v N_i^T M_i^{1/2}}{\left( \frac{\mu D_m^K}{B_k P} + \sum_{i=1}^v X_i M_i^{1/2} \right)}, \quad (8)$$

where  $M_i$  is the molecular weight of gas  $i$ , and an intrinsic Knudsen diffusivity,  $D_m^K \equiv D_i^K M_i^{1/2}$ , can be used in place of individual  $D_i^K$ .

A value for the permeability,  $B_k$ , is needed in Eq. (8). From Fig. 4, the steady-state pressure difference at the transducers is  $-4 \pm 1$  Pa through the 30-cm sand column at a  $CO_2$  flux of  $11,200 \text{ g m}^{-2} \text{ day}^{-1}$ . However, pressures with gas flow give only an apparent permeability ( $B_{ka}$ ) using Darcy's law:  $B_{ka} = -N^T \mu RT / P \nabla P$ . While the net molar gas flux ( $-N^T$ ) is constant at all depths and equal to  $255 \text{ mol m}^{-2} \text{ day}^{-1}$ , gas composition, and therefore  $\mu$ , is not constant. The change in gas composition with depth also means that the four transducer tubes are filled with gas mixtures of different molecular weights. Thus, the pressure gradient sensed by the transducers not only reflects the difference in head, but also the gravitational effects on the gas in the connecting tubes. Gravitational effects are not negligible at such small pressure gradients, although Thorstenson and Pollock (1989a) have shown that they need not be explicitly included in Eq. (8). Here, we are fortunate that the interval between 20 and 30 cm depth, and presumably both transducer tubes, contained almost

pure CO<sub>2</sub>. Thus, the measured  $\Delta P$  ( $-2 \pm 0.5$ Pa) results entirely from a difference in head. For distinction, this component of pressure, which is the driving force for viscous flux, can be denoted  $P'$ , and  $\nabla P'$  is, therefore,  $-20$  Pa/m. Also,  $\mu$  can be considered constant through this interval and equal to  $\mu_{\text{CO}_2}$ , so:

$$B_{\text{ka}} = -N_{\text{CO}_2}^T \mu_{\text{CO}_2} RT / (P \nabla P') = 52 \text{ darcies.} \quad (9)$$

The intrinsic permeability,  $B_k$ , can be calculated from:

$$B_{\text{ka}} \equiv B_k [1 + (b_i/P)], \quad (10)$$

and:

$$b_i = D_i^K \mu_i / B_k, \quad (11)$$

where  $b_i$ , the Klinkenberg parameter, is a characteristic of the porous medium, its water content (Stonestrom and Rubin, 1989), and gas  $i$ , in this case, CO<sub>2</sub>. An intrinsic Klinkenberg parameter can also be defined (Thorstenson and Pollock, 1989a):

$$b_m \equiv b_i M_i^{1/2} / \mu_i = D_m^K / B_k. \quad (12)$$

We did not measure  $b_i$ . However, Abu-El-Sha'r and Abriola (1997) recently reported several values of  $D_i^K$ ,  $B_{\text{ka}}$  and  $B_k$  for 30-mesh, dry sea sand. They used variable packing to achieve four porosities between 0.39 and 0.46 and the respective  $B_{\text{ka}}$  values (with helium) from 25 to 79 darcies, a range that cover the conditions of the sand in our tests. Over this range of  $n_a$  and  $B_{\text{ka}}$ , Abu-El-Sha'r and Abriola (1997) report  $D_{\text{He}}^K / B_k$  values of  $1.3 \pm 0.2 \times 10^9$ . This gives a  $D_m^K / B_k$  of  $2.6 \times 10^9$ , which we can use in Eq. (12) to obtain a  $b_{\text{CO}_2}$  of  $0.44 \times 10^4$  Pa. Using that value in Eq. (10) gives a  $B_k$  of 50 darcies for our sand.

Although the difference between  $B_{\text{ka}}$  and  $B_k$ , in this case, is much smaller than the uncertainty in either value, this might not be true in very fine-grained or water-rich media (Stonestrom and Rubin, 1989; Severinghaus et al., 1996). Regardless, it is the  $D_m^K / B_k$  ( $= b_m$ ) value that allows the viscous flux to be calculated using Eq. (8). Again, CO<sub>2</sub> is the only nonstagnant gas, so:

$$\sum_{i=1}^v N_i^T M_i^{1/2} = N_{\text{CO}_2}^T M_{\text{CO}_2}^{1/2} = 6.633 N^T \quad (13)$$

For our purposes, it is useful to consider the viscous fraction of the net (or total) molar flux. To calculate this fraction,  $N^V / N^T$ , Eq. (8) can be recast as:

$$\frac{N^V}{N^T} = \frac{6.633}{\left( \frac{\mu b_m}{P} + \sum_{i=1}^v X_i M_i^{1/2} \right)}. \quad (14)$$

In order to calculate the viscous flux throughout the sand column,  $\mu$  is approximated by:

$$\mu = \sum_{i=1}^v X_i \mu_i. \quad (15)$$

Because all  $X_i$  can be expressed as a function of [CO<sub>2</sub>] using Eq. (7),  $N^V / N^T$  and all  $N_i^V / N^T$  ( $= X_i N^V / N^T$ ) can also be expressed as a function of [CO<sub>2</sub>], independent of depth and total flux.

Some of these flux ratios are plotted in Fig. 9, which allows the ratios to be easily calculated at any point on a CO<sub>2</sub> profile. For example, at the bottom of the  $12,400 \text{ g m}^{-2} \text{ day}^{-1}$  profile, the gas is essentially 100% CO<sub>2</sub> (Fig. 6). From Fig. 9, 95% of the CO<sub>2</sub> is transported by viscous flux. At the sand surface, only about 2% of the CO<sub>2</sub> transport is viscous, and the rest, diffusive. However, Fig. 9 shows that the combined viscous flux of all gas species actually increases to 114% of the total flux. This result is possible because the greater velocity of the air molecules relative to the heavier, slower CO<sub>2</sub>

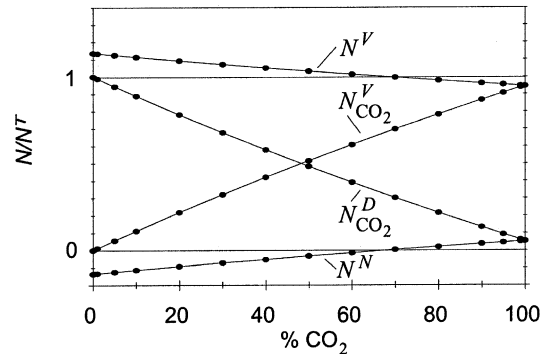


Fig. 9. Ratio of various flux components to net or total molar flux ( $N^T$ ) calculated using Eq. (14).  $N^V$  is the net viscous flux of all gas species;  $N_{\text{CO}_2}^V$  is the viscous flux of CO<sub>2</sub>.  $N^N$  is the net diffusive flux of all species;  $N_{\text{CO}_2}^D$  is the diffusive flux of CO<sub>2</sub>. Note that  $N^T$  is negative (out of the sand) as are all other fluxes shown except  $N^N$ .

leads to a small net diffusive flux of gas (the nonequimolar flux,  $N^N$ ) into the sand that must be exactly balanced by an increase in the viscous efflux. The gradient in pressure (head),  $\nabla P'$ , associated with viscous flux can also be calculated as a function of  $[\text{CO}_2]$  using Fig. 9.

All our tests used pure  $\text{CO}_2$  at the inlet, and for this case, Fig. 9 shows that percentage of  $\text{CO}_2$  transported by viscous flux at each depth is approximately equal to its concentration at that depth. A similar relation could hold in natural high-flux areas when soils are dry, but not necessarily in field areas characterized by an unusually large ratio of  $b_m/P$  (e.g., very fine-grained soil at high altitude). Strict application of Fig. 9 and the transport equations herein also requires that the abiogenic  $\text{CO}_2$  flux heavily predominate over both the soil respiration fluxes and any net air fluxes that might arise from diurnal barometric cycles and/or orographic effects (see, e.g., Weeks, 1987, 1993). In cases where air cannot be considered a stagnant gas or in thermal areas where steam transport is significant, more complex transport equations should be considered (e.g., Massmann and Farrier, 1992). In any case, viscous flux is likely to be the biggest component of total gas flux across the soil surface when  $\text{CO}_2$  is derived from deep geologic processes.

#### 5.4. Accumulation chamber effects

Even though  $\text{CO}_2$  transport is nearly all diffusive near the sand surface, an accumulation chamber set on that surface still encounters a large viscous flow of gas (mainly) air and, therefore, a pressure gradient. Gas pressure gradients can exist in all soil environments, but the low net fluxes normally associated with respiration may allow an accumulation chamber to be placed on the soil without seriously altering that gradient. At the high fluxes of interest here, the effect of the chamber on the pressure gradient must be considered. The one-dimensional, steady-state, modeling presented here can illustrate, but not quantify, this effect.

As an example, one of the chambers tested here was 10 cm high with a  $0.053 \text{ m}^2$  footprint. Consider flux measurement at the  $1900 \text{ g m}^{-2} \text{ day}^{-1}$  rate, a net molar flux ( $-N^T$ ) of  $5.00 \times 10^{-4} \text{ mol m}^{-2} \text{ s}^{-1}$ . Near the top of the sand where  $X_{\text{CO}_2}$  is low (0.0026

in Fig. 6), Fig. 9 shows that  $N^V/N^T = 1.14$ . Thus,  $-N^V = 5.70 \times 10^{-4} \text{ mol m}^{-2} \text{ s}^{-1}$ . From Darcy's law  $\nabla P' = N^V \mu RT / B_k P = -5.0 \text{ Pa/m}$ . At the laboratory pressure ( $1.01 \times 10^5 \text{ Pa}$ ) and temperature (293 K),  $5.00 \times 10^{-4} \text{ mol}$  gas occupies  $1.2 \times 10^{-5} \text{ m}^3$ , so  $-N^T$  corresponds to a gas velocity of  $0.0012 \text{ cm s}^{-1}$  in free space and  $0.0030 \text{ cm s}^{-1}$  in the sand with  $n_a = 0.4$ . Undisturbed, this net flux would cause a hypothetical pressure increase within the chamber of 12 Pa in just the first second after emplacement, clearly impossible given that the steady-state  $\Delta P'$  across a 0.0030-cm thickness of sand is only 0.00015 Pa. Therefore, net gas flux is almost totally diverted out under the edges of the chamber in that initial second, a change probably too rapid to be detected in a  $d[\text{CO}_2]/dt$  plot.

An identical chamber was equipped with a vent tube 3 mm in I.D. Again assuming an undisturbed net flux, the  $2.6 \times 10^{-5} \text{ mol s}^{-1}$  ( $0.053 \text{ m}^2 \times -N^T$ ) entering the chamber would create a flux through the vent tube of  $3.7 \text{ mol m}^{-2} \text{ s}^{-1}$ . The  $\Delta P'$  across the 3-cm-long tube can be estimated from Poiseuille's law ( $-N = r^2 P \nabla P / 8 \mu RT$ ) as:

$$(0.03)(3.7)(8 \mu RT / r^2 P) = 0.17 \text{ Pa}, \quad (16)$$

which is still three orders of magnitude greater than the steady-state  $\Delta P'$  across the top 0.0030 cm of sand. For this particular chamber, the pressure drop calculated in Eq. (16) is equal to the steady-state  $\Delta P'$  in the upper 3 cm of sand. This calculation may explain why plugging this vent tube made no discernible difference in the measured fluxes. An accumulation chamber, vented or not, presents an immediate and almost total barrier to net gas flux.

Although net gas flux is blocked and diverted by the chamber, the diffusive efflux of  $\text{CO}_2$  into the chamber continues, in balance with diffusive flux of air into the medium. Because the steady-state  $\text{CO}_2$  transport across the interface is almost entirely diffusive ( $\sim 99\%$ ) before the chamber is set, the blockage of net flux might initially be presumed to have little impact on  $\text{CO}_2$  efflux. However, the linkage between  $\nabla P'$  and  $\nabla \text{CO}_2$  in a porous medium requires that diffusive efflux of  $\text{CO}_2$  adjust for the large change in pressure gradients. We propose that this adjustment is the reason that measured fluxes were 12.5%, rather than  $\sim 1\%$ , lower than imposed fluxes.

Some chamber effects were demonstrated experimentally. Fig. 10 shows the measured  $[\text{CO}_2]$  profiles underneath the center of the above-mentioned chamber before and after a 2-min flux measurement. Prior to setting the chamber, the profile above the surface is not known and might be highly variable, but is approximated by a dashed line between the two measured points (in this case, 0.05% at +10 cm and 0.42% at 0 cm). After the chamber is placed with fan running, the  $[\text{CO}_2]$  above the sand should be uniform (vertical profile). During the 2-min run, the  $[\text{CO}_2]$  in the chamber reached 2.0%, while the  $[\text{CO}_2]$  increased by 1.5% at 2.5 cm depth and by 0.8% at 4 cm depth. At 6 cm depth and below, differences were less than measurement uncertainty. On the “after” profile, the dashed section indicates that the  $[\text{CO}_2]$  at the interface is unknown.

The  $d[\text{CO}_2]/dt$  plot is shown in Fig. 11. The chamber was set down at  $t \sim 15$  s, containing normal air ( $[\text{CO}_2] = 0.036\%$ ). Very quickly, the  $[\text{CO}_2]$  rose to the “ambient” value, 0.05%, for  $z = +10$  cm. About 20 s later, the interfacial ambient  $[\text{CO}_2]$ , 0.42%, was reached. At about 0.9%  $\text{CO}_2$ ,  $\sim 50$  s after chamber emplacement, the  $d[\text{CO}_2]/dt$  plot began to show visible curvature. In repeated tests, where the gas detectors were continuously running, a  $[\text{CO}_2]$  buildup of several tenths of a percent could be detected at 2.5 cm depth 50 s into a run, and a small increase ( $\sim 0.1\%$ ) could be detected at 4 cm depth. These findings thus support the assertion of Chiodini et al. (1998) that  $d[\text{CO}_2]/dt$  is initially straight at high fluxes, but also show that some  $\text{CO}_2$  builds up

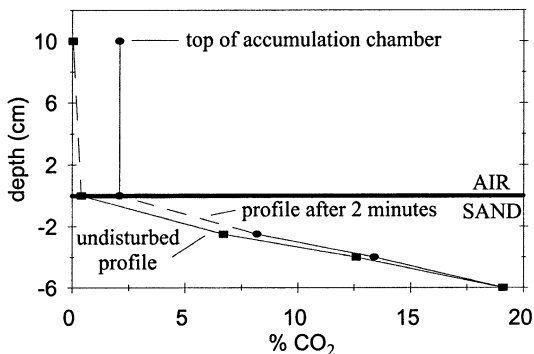


Fig. 10. Profiles of  $[\text{CO}_2]$  before and after a 2-min flux measurement at  $1900 \text{ g m}^{-2} \text{ day}^{-1}$  using a 10-cm-high accumulation chamber. Dashed portions are assumed.

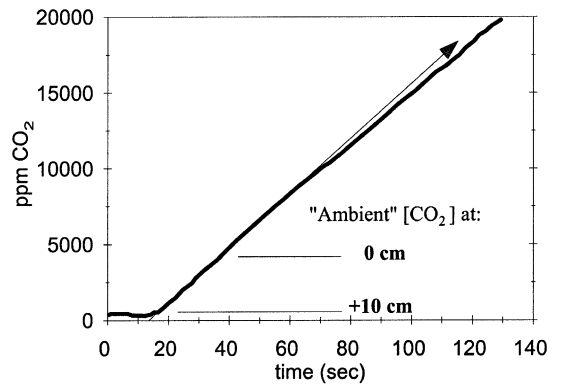


Fig. 11. Plot of  $d[\text{CO}_2]/dt$  measured as in Fig. 10 (heavy line). Two possible choices of ambient  $[\text{CO}_2]$  are shown based on gas meter readings taken before the chamber was emplaced. Plot shows curvature (relative to arrow) beginning about 50 s after emplacement.

beneath the chamber even during this initial straight part of the  $d[\text{CO}_2]/dt$  plot. Our measurements are too few and imprecise to determine conclusively if this “chamber effect” is sufficient to account for the fact that the flux calculated from the initial slope of the  $d[\text{CO}_2]/dt$  plot in this test was 11% less than the imposed flux, but are highly suggestive of a negative bias in accumulation chamber techniques.

Figs. 10 and 11 also illustrate another problem that arises under high flux conditions: the uncertainty in defining “ambient”  $[\text{CO}_2]$ . Because a sizable  $[\text{CO}_2]$  gradient forms above the sand surface, there is no unambiguous choice of where to pick  $d[\text{CO}_2]/dt$  for Eq. (1). This further suggests that pre-scrubbing the chamber is not necessarily a benefit. Certainly, pre-scrubbing will not reduce the impact of the chamber on pressure gradients.

## 6. Conclusions

In a laboratory test system designed to simulate a natural coarse-grained soil, accumulation chambers proved capable of measuring imposed  $\text{CO}_2$  fluxes up to at least  $10^4 \text{ g m}^{-2} \text{ day}^{-1}$ , > 95% of all measurements were within 25% of imposed fluxes. This level of accuracy would seem to be acceptable for many geological investigations of volcanoes and faults. In contrast to soil-respiration fluxes, imposed  $\text{CO}_2$

fluxes (e.g., from buried sources such as magma or metamorphic decarbonation) result in large net effluxes of gas at the surface, and it appears that accumulation chambers, even if vented, block almost all net gas flow into the chamber. The restriction of the net efflux of gas alters both the pressure and concentration gradients, and is ultimately the most likely reason that CO<sub>2</sub> fluxes measured in these tests were 12.5% low on average.

Studies in high-CO<sub>2</sub> flux areas frequently include an investigation of soil–gas chemistry and isotopes in an effort to determine gas sources. However, fractionations related to diffusive transport through the soil are seldom considered. The results obtained in these tests demonstrate the large magnitude of possible fractionations that may obscure or overwhelm the chemical or isotopic signatures of the sources. One procedure to help sort out gas data from well-characterized soils would be to compare measured concentration profiles with results predicted by Eq. (6). In general, Eq. (7) may be more useful than Eq. (6) for comparing soil–gas compositions and isotopic values from different types of soils and seems capable of handling simple compounds with molecular masses between 4 and 132. The value of using the noble gas suite in transport studies is made obvious by the eightfold enrichment in <sup>4</sup>He/<sup>132</sup>Xe observed in the 80% CO<sub>2</sub> sample (Table 1), relative to abundancies in air. Our results at least show that gas samples collected by either sudden (pre-evacuated container) or gradual (gas pump) removal of tens of cm<sup>3</sup> of gas through an access pipe appear to reflect steady-state values.

On-site measurements other than CO<sub>2</sub> flux could add much to the study of high-flux areas. In particular, obtaining simultaneous measurements of pressure and CO<sub>2</sub> gradients together with flux would be well worth the effort.

### Acknowledgements

Other researchers who contributed flux measurements reported above were Deb Bergfeld, Tanvir Demetriades-Shah (LI-COR), Chris Farrar, Terry Gerlach, Jen Lewicki, Ken McGee and John Neil. Kathy Akstin and L. Doug White provided analytical help. Don Thorstenson and Ed Weeks provided help-

ful information and discussions. We acknowledge Bill Herkelrath, Yousif Kharaka, Sue Brantley and Ken Wohletz for reviews. This work was partly supported by the Director, Office of Energy Research, Office of Basic Energy Sciences, Engineering and Geoscience Division of the U.S. Department of Energy under contract DE-AC03-76SF00098.

### References

- Abu-El-Sha'r, W., Abriola, L.M., 1997. Experimental assessment of gas transport mechanisms in natural porous media: parameter evaluation. *Water Resour. Res.* 33, 505–516.
- Allard, P., Carbonelle, J., Dajlevic, D., Le Bronec, J., Morel, P., Robe, M.C., Maurenas, J.M., Faivre-Pierret, R., Martin, D., Sabroux, J.C., Zettwoog, P., 1991. Eruptive and diffuse emissions of CO<sub>2</sub> from Mount Etna. *Nature* 351, 387–391.
- Anthony, W.H., Hutchinson, G.L., Livingston, G.P., 1995. Chamber measurement of soil–atmosphere gas exchange: linear vs. diffusion-based flux models. *Soil Sci. Soc. Am. J.* 59, 1308–1310.
- Badalamenti, B., Gurrieri, S., Hauser, S., Parello, F., Valenza, M., 1988. Soil CO<sub>2</sub> output in the island of Vulcano during the period 1984–1988: surveillance of gas hazard and volcanic activity. *Rend. Soc. Ital. Mineral. Petrol.* 43, 893–899.
- Baubron, J.C., Allard, P., Toutain, J.P., 1990. Diffuse volcanic emissions of carbon dioxide from Vulcano Island, Italy. *Nature* 344, 51–53.
- Bergfeld, D., Goff, F., Janik, C.J., 1998. CO<sub>2</sub> flux measurements at the Dixie Valley geothermal system, Nevada. *EOS* 79F, 941.
- Chiodini, G., Marini, L., 1998. Hydrothermal gas equilibria: the H<sub>2</sub>O–H<sub>2</sub>–CO<sub>2</sub>–CO–CH<sub>4</sub> system. *Geochim. Cosmochim. Acta* 62, 2673–2687.
- Chiodini, G., Cioni, R., Guidi, M., Raco, B., Marini, L., 1998. Soil CO<sub>2</sub> flux measurements in volcanic and geothermal areas. *Appl. Geochem.* 13, 543–552.
- Chiodini, G., Frondini, F., Kerrick, D.M., Rogie, J., Parello, F., Peruzzi, L., Zanzari, A.R., 1999. Quantification of deep CO<sub>2</sub> fluxes from Central Italy. Examples of carbon balance for regional aquifers and of soil diffuse degassing. *Chem. Geol.* 159, 205–222.
- Currie, J.A., 1970. Movement of gases in soil respiration. Sorption and Transport Processes in Soils. *Monogr. Soc. Chem. Ind.*, vol. 37, pp. 152–171.
- Evans, W.C., White, L.D., Rapp, J.B., 1988. Geochemistry of some gases in hydrothermal fluids from the southern Juan de Fuca Ridge. *J. Geophys. Res.* 93, 15305–15313.
- Evans, W., Sorey, C., Michel, L., Kennedy, L., Hainsworth, M., 1998. Gas–water interaction at Mammoth Mountain, California, USA. In: Balkema, A.A. (Ed.), *Proc. 9th International Symposium on Water–Rock Interaction*, Rotterdam, 1998. pp. 443–446.

- Farrar, C.D., Sorey, M.L., Evans, W.C., Howle, J.F., Kerr, B.D., Kennedy, B.M., King, C.Y., Southon, J.R., 1995. Forest-killing diffuse CO<sub>2</sub> emission at Mammoth Mountain as a sign of magmatic unrest. *Nature* 376, 675–678.
- Farrar, C.D., Neil, J.M., Howle, J.F., 1998. Magmatic carbon dioxide emissions at Mammoth Mountain, California. U.S. Geol. Surv. Water Resour. Invest. Rep. 98-4217, 34 pp.
- Gerlach, T.M., Doukas, M.P., McGee, K.A., Kessler, R., 1998. Three-year decline of magmatic CO<sub>2</sub> emissions from soils of a Mammoth Mountain tree kill: Horseshoe Lake, CA, 1995–1997. *Geophys. Res. Lett.* 25, 1947–1950.
- Giammanco, S., Gurrieri, S., Valenza, M., 1998. Anomalous soil CO<sub>2</sub> degassing in relation to faults and eruptive fissures on Mount Etna (Sicily, Italy). *Bull. Volcanol.* 60, 252–259.
- Gurrieri, S., Valenza, M., 1988. Gas transport in natural porous mediums: a method for measuring CO<sub>2</sub> flows from the ground in volcanic and geothermal areas. *Rend. Soc. Ital. Mineral. Petrol.* 43, 1151–1158.
- Healy, R.W., Striegl, R.G., Russell, T.F., Hutchinson, G.L., Livingston, G.P., 1996. Numerical evaluation of static-chamber measurements of soil–atmosphere gas exchange: identification of physical processes. *Soil Sci. Soc. Am. J.* 60, 740–747.
- Hiyagon, H., Kennedy, B.M., 1992. Noble gases in CH<sub>4</sub>-rich gas fields, Alberta, Canada. *Geochim. Cosmochim. Acta* 56, 1569–1589.
- Kennedy, B.M., Lynch, M.A., Reynolds, J.H., Smith, S.P., 1985. Intensive sampling of noble gases in fluids at Yellowstone: I. Early overview of the data: regional patterns. *Geochim. Cosmochim. Acta* 49, 1251–1261.
- Kestin, J., Yata, J., 1968. Viscosity and diffusion coefficient of six binary mixtures. *J. Chem. Phys.* 49, 4780–4791.
- Marrero, T.R., Mason, E.A., 1972. Gaseous diffusion coefficients. *J. Phys. Chem. Ref. Data* 1, 3–118.
- Mason, E.A., Malinauskas, A.P., Evans III, R.B., 1967. Flow and diffusion of gases in porous media. *J. Chem. Phys.* 46, 3199–3216.
- Massmann, J., Farrier, D.F., 1992. Effects of atmospheric pressures on gas transport in the vadose zone. *Water Resour. Res.* 28, 777–791.
- McGee, K.A., Gerlach, T.M., 1998. Annual cycle of magmatic CO<sub>2</sub> in a tree-kill soil at Mammoth Mountain, California: implications for soil acidification. *Geology* 26, 463–466.
- Minissale, A., Evans, W.C., Magro, G., Vaselli, O., 1997. Multiple source components in gas manifestations from north-central Italy. *Chem. Geol.* 142, 175–192.
- Nay, S.M., Mattson, K.G., Bormann, B.T., 1994. Biases of chamber methods for measuring soil CO<sub>2</sub> efflux demonstrated with a laboratory apparatus. *Ecology* 75, 2460–2463.
- Norman, J.M., Kucharik, C.J., Gower, S.T., Baldocchi, D.D., Crill, P.M., Rayment, M., Savage, K., Striegl, R.G., 1997. A comparison of six methods for measuring soil–surface carbon dioxide fluxes. *J. Geophys. Res.* 102, 28771–28777.
- Perry, R., Green, H., 1984. *Perry's Chemical Engineers' Handbook*. 6th edn. McGraw-Hill, New York, p. 2100.
- Severinghaus, J.P., Bender, M.L., Keeling, R.F., Broecker, W.S., 1996. Fractionation of soil gases by diffusion of water vapor, gravitational settling, and thermal diffusion. *Geochim. Cosmochim. Acta* 60, 1005–1018.
- Sorey, M.L., Evans, W.C., Kennedy, B.M., Farrar, C.D., Hainsworth, L.J., Hausback, B., 1998. Carbon dioxide and helium emissions from a reservoir of magmatic gas beneath Mammoth Mountain, California. *J. Geophys. Res.* 103, 15303–15323.
- Stonestrom, D.A., Rubin, J., 1989. Air permeability and trapped-air content in two soils. *Water Resour. Res.* 25, 1959–1969.
- Thorstenson, D.C., Pollock, D.W., 1989a. Gas transport in unsaturated zones: multicomponent systems and the adequacy of Fick's laws. *Water Resour. Res.* 25, 477–507.
- Thorstenson, D.C., Pollock, D.W., 1989b. Gas transport in unsaturated porous media: the adequacy of Fick's law. *Rev. Geophys.* 27, 61–78.
- Weeks, E., 1987. Effect of topography on gas flow in unsaturated fractured rock: concepts and observations. In: Evans, D., Nicholson, D. (Eds.), *Flow and Transport Through Unsaturated Fractured Rock*. *Geophys. Monogr. Ser.* 42 AGU, Washington, DC, pp. 165–170.
- Weeks, E., 1993. Does the wind blow through Yucca Mountain? In: Evans, D., Nicholson, D. (Eds.), *Proceedings of Workshop V: Flow and Transport Through Unsaturated Fractured Rock-Related to High-Level Radioactive Waste Disposal*. U.S. Nucl. Reg. Comm., [Rep.] NUREG/CP-0040, pp. 43–53.
- Welles, J.M., Demetriades-Shah, T., McDermitt, D.K., 2000. Considering for measuring ground CO<sub>2</sub> fluxes with chambers (this volume).
- Werner, C.A., Bailey, D., Voigt, D.E., Brantley, S.L., 1998. Temporal and spatial variability of CO<sub>2</sub> fluxes in the Mud Volcano thermal area of Yellowstone National Park, WY. *EOS* 79F, 941.
- Wood, J.T., Greenwood, D.J., 1971. Distribution of carbon dioxide and oxygen in the gas phase of aerobic soils. *J. Soil Sci.* 22, 281–288.
- Wood, W.W., Petraitis, M.J., 1984. Origin and distribution of carbon dioxide in the unsaturated zone of the Southern High Plains of Texas. *Water Resour. Res.* 20, 1193–1208.